CMS Physics Analysis Summary

Contact: cms-pag-conveners-b2g@cern.ch 2018/03/22

Search for a heavy resonance decaying into a vector boson and a Higgs boson in semileptonic final states at $\sqrt{s} = 13$ TeV

The CMS Collaboration

Abstract

A search for heavy resonances decaying into a vector boson and the standard model Higgs boson is presented, in final states containing b quark-antiquark pairs from the decay of the Higgs boson and leptons (electrons and muons) or missing transverse momentum, because of undetected neutrinos, from the decay of the vector bosons. The analysis is performed using a data sample corresponding to an integrated luminosity of 35.9 fb^{-1} collected in 2016 by the CMS experiment at the CERN LHC from proton-proton collisions at a center-of-mass energy of 13 TeV. The data are found to be consistent with the background expectations. Exclusion limits are set in the context of spin-1 heavy vector resonances and spin-0 two Higgs doublet models, also including the presence of dark matter. In a model with heavy vector triplet, W′ and Z′ resonances with a degenerate mass smaller than 2.9 TeV are excluded at 95% confidence level if the couplings to the standard model bosons dominate.

1 Introduction

The discovery of a Higgs boson at the CERN LHC [1–3] and the measurement of its mass and quantum numbers [4–7] consolidates the standard model (SM) of particle physics. Although the SM provides reliable and accurate predictions of observables at energies up to the TeV scale, the relatively light mass of the Higgs boson of 125 GeV [7] indicates either a large amount of fine tuning or the presence of new heavy particles, denoted as X, above the electroweak (EW) scale [8]. The relation between these heavy particles and the EW and Higgs sectors of the SM suggests that the new resonances may decay with a significant branching fraction into a SM vector boson (W or Z) and a Higgs boson (h).

Several extensions of the SM with extra $\mathrm{SU}(2)$ or $\mathrm{U}(1)$ gauge groups, such as minimal W′ and Z′ models, strongly coupled composite Higgs models, and little Higgs models, postulate the existence of massive gauge bosons (W′ and Z′) with weak couplings to the SM particles [9–18]. A large number of these models are described by the heavy vector triplet (HVT) framework [19], which extends the SM by introducing a triplet of heavy vector bosons, one neutral (Z′) and two electrically charged ($\mathrm{W'}^{\pm}$), which are degenerate in mass and are collectively referred to as V′. In the HVT framework, g_V is the coupling strength of the new interaction, c_H is the coupling coefficient between the HVT bosons, the Higgs boson, and longitudinally polarized SM vector bosons, c_F is the coupling coefficient between the HVT bosons and the SM fermions, and g is the SM $\mathrm{SU}(2)_\mathrm{L}$ gauge coupling. The coupling strength of the heavy vector bosons to SM bosons and fermions is determined by the $g_\mathrm{V} c_\mathrm{H}$ and $g^2 c_\mathrm{F}/g_\mathrm{V}$ parameters, respectively. The HVT framework is presented in two scenarios, henceforth referred to as model A and model B, depending on the couplings to the SM particles [19]. In model A ($g_\mathrm{V} = 1$, $c_\mathrm{H} = -0.556$, $c_\mathrm{F} = -1.316$), the coupling strengths to the SM bosons and fermions are comparable and the new particles decay primarily to fermions, as predicted by Z′ and W′ models. In model B ($g_\mathrm{V} = 3$, $c_\mathrm{H} = -0.976$, $c_\mathrm{F} = 1.024$), such as the composite Higgs models, the branching fraction to the SM bosons is nearly 100% since the couplings to the SM fermions are small.

Heavy spin-0 resonances are also predicted in extensions of the SM Higgs sector, like two Higgs doublet models (2HDM) [20], which introduce a second scalar doublet in addition to the one from the SM. Different formulations of 2HDM predict different couplings of the two doublets to quarks and to massive leptons. In Type-I 2HDM, all fermions couple to only one Higgs doublet, while in Type-II, the up- and down-type quarks couple to different doublets. The two Higgs doublets entail the presence of five physical states: two neutral and CP-even bosons (h and H, the latter being more massive) a neutral and CP-odd boson (A), and two charged scalar bosons ($\mathrm{H}^{\pm}$). Depending on the model free parameters $\tan\beta$ and α, which are the ratio of the vacuum expectation values, and the mixing angle of the two Higgs doublets, respectively, the dominant A boson production process can be either through gluon-gluon fusion or through b quark associated production, as shown in Fig. 1. In both cases, the heavy pseudoscalar boson A may decay with a large branching fraction to a pair of Z and h bosons [20].

A particular formulation of the two Higgs doublet model, denoted as Z′-2HDM model [21, 22], is obtained by extending the 2HDM with an additional $\mathrm{U}(1)_{Z'}$ symmetry group which postulates a heavy spin-1 Z′ particle with gauge coupling $g_{Z'}$, and a candidate for dark matter (DM), denoted as χ, which couples to the A boson with coupling strength g_χ. In the process considered in this search, the Z′ is produced from $\mathrm{q\bar{q}}$ annihilation and decays into a pseudoscalar A boson and a light Higgs boson. The Higgs boson decays to a b quark-antiquark pair ($\mathrm{b\bar{b}}$), and the A boson decays into a pair of DM particles ($\chi\bar{\chi}$), which escape the detection making this signature kinematically indistinguishable from the $\mathrm{Z'} \to \mathrm{Zh} \to \nu\nu\mathrm{b\bar{b}}$ signal. The Feynman diagram of this process is reported in Fig. 1.

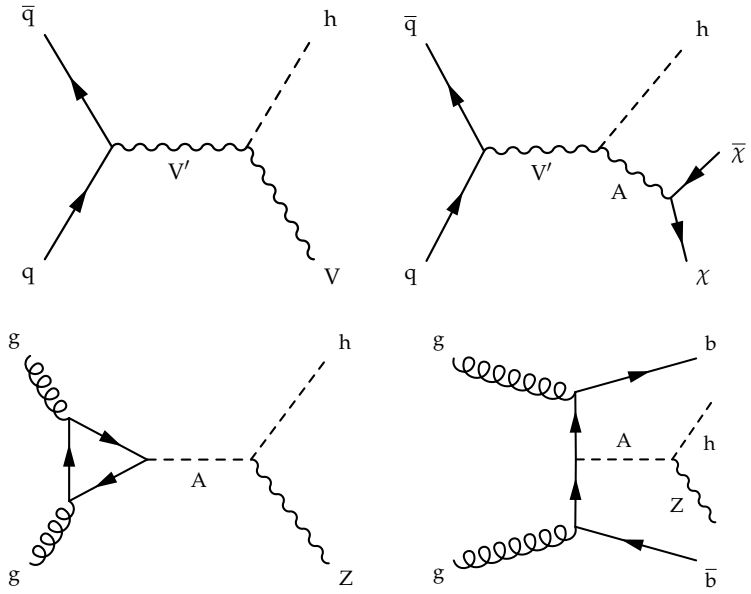

Figure 1: Feynman diagrams of the considered processes: heavy spin-1 vector boson production and decay to a SM vector boson and a Higgs boson, as in the HVT framework (upper left); Z′ boson that decays to a Higgs boson and a A boson, with the latter decaying into dark matter particles ($\chi\overline{\chi}$), predicted by the Z′-2HDM model (upper right); production within the 2HDM model of a pseudoscalar A boson through gluon-gluon fusion (lower left) and with accompanying b quarks (lower right).

Previous ATLAS and CMS searches indicate that the mass of the resonance m_X should exceed 1 TeV [23–35]. Hence, the V and h bosons originating from its decay have a large Lorentz boost, and thus the $h \to b\bar{b}$ is reconstructed using a single jet containing the collimated decay products of the two hadronized b quarks.

This article describes a search on proton-proton (pp) collisions at a center-of-mass energy of 13 TeV collected by the CMS experiment at the LHC during 2016 for heavy resonances decaying into a vector boson (W or Z) and a Higgs boson. The SM Higgs boson is assumed to decay to a $b\bar{b}$ pair with a branching fraction of 58% [36], and the vector boson in final states with 0, 1, or 2 charged leptons ($Z \to \nu\nu$, $W \to \ell\nu$, $Z \to \ell\ell$).

This search is complementary to the CMS analysis targeting hadronic vector boson decays [30] that excludes HVT triplets up to 3.1 and 3.3 TeV in model A and B, respectively, and retains a better sensitivity especially at low m_X thanks to the leptonic vector boson decays. This result significantly extends the sensitivity of the CMS searches in the same final state performed with 2.2–2.5 fb^{-1} of data collected during 2015, which excluded a V′ boson with mass below 2.0 TeV in the HVT model B [27], and a $m_{Z'} < 1.8$ TeV and $m_A < 500$ GeV in the Z′-2HDM model [34].

2 CMS detector

A detailed description of the CMS detector, together with a definition of the coordinate system used and the relevant kinematic variables, can be found in Ref. [37].

The central feature of the CMS apparatus is a superconducting solenoid of 6 m internal diameter, providing a magnetic field of 3.8 T. Within the solenoid volume are a silicon pixel and strip tracker, a lead tungstate crystal electromagnetic calorimeter (ECAL), and a brass and scintilla-

tor hadron calorimeter (HCAL), each composed of a barrel and two endcap sections. Forward calorimeters extend the pseudorapidity coverage provided by the barrel and endcap detectors. Muons are detected in gas-ionization chambers embedded in the steel flux-return yoke outside the solenoid.

The silicon tracker measures charged particles within the pseudorapidity range $|\eta| < 2.5$. It consists of 1440 silicon pixel and 15 148 silicon strip detector modules. For nonisolated particles with transverse momenta of $1 < p_T < 10$ GeV and $|\eta| < 1.4$, the track resolutions are typically 1.5% in p_T and 25–90 (45–150) μm in the transverse (longitudinal) impact parameter [38]. The ECAL provides coverage up to $|\eta| < 3.0$, and the energy resolution for unconverted or late-converting electrons and photons in the barrel section is about 1% for particles that have energies in the range of tens of GeV. The dielectron mass resolution for $Z \to ee$ decays when both electrons are in the ECAL barrel is 1.9%, and is 2.9% when both electrons are in the endcaps. The HCAL covers the range of $|\eta| < 3.0$, which is extended to $|\eta| < 5.2$ through forward calorimetry. Muons are measured in gas-ionization detectors embedded in the steel flux-return yoke outside the solenoid, and cover the pseudorapidity range $|\eta| < 2.4$. The muon detectors make use of three different technologies: drift tubes, cathode strip chambers, and resistive-plate chambers. Combining muon tracks with matching tracks measured in the silicon tracker results in a p_T resolution of 2–10% for muons with $0.1 < p_T < 1$ TeV [39].

The first level of the CMS trigger system [40], composed of custom hardware processors, uses information from the calorimeters and muon detectors to select the most interesting events in a fixed time interval of less than 4 μs. The high-level trigger (HLT) processor farm decreases the event rate from around 100 kHz to about 1 kHz, before data storage.

3 Data and simulated samples

The data sample analyzed in this search corresponds to an integrated luminosity of 35.9 fb^{-1}, collected with the CMS detector at the LHC in ppcollisions at a center-of-mass energy of 13 TeV.

The spin-1 gauge bosons W′ and Z′ are simulated according to the HVT model B parameters at leading order (LO) using MADGRAPH5_aMC@NLO [19]. Different m_X hypotheses in the range 800 to 4500 GeV are considered, assuming a resonance width narrow enough (0.1% of the resonance mass) to be negligible compared to the experimental resolution. This assumption is valid in a large fraction of the HVT parameter space, and fulfilled in both benchmark models A and B [19].

The spin-0 signal is generated at LO with MADGRAPH5_aMC@NLO in both the gluon-gluon fusion and b quark associated production processes according to the 2HDM model [20], assuming a narrow signal width. In the gluon fusion production mode, up to one additional jet is included in the final state, and only the top quark runs in the loop reported in Fig. 1. The $A \to Zh$ decay is simulated with MADSPIN.

The Z′-2HDM signal is generated at LO with MADGRAPH5_aMC@NLO assuming $g_{Z'} = 0.8$, an unitary coupling of the A boson to the DM candidate ($g_\chi = 1$) and $\tan\beta = 1$, and the heavy Higgs bosons are degenerate in mass [41]. In the case where $\cos(\beta - \alpha) \to 0$, denoted as alignment limit, the light Higgs boson is virtually indistinguishable from the SM Higgs boson, and the Higgs boson branching fractions match the ones of the SM. This signal is characterized by the masses $m_{Z'}$ and m_A, while the mass of the DM candidate m_χ does not affect the kinematic distributions significantly if the A boson is on-shell. The DM candidate mass is therefore set to a fixed value $m_\chi = 100$ GeV while $m_{Z'}$ is varied between 800 and 4000 GeV, and m_A between

300 and 800 GeV [41].

The SM backgrounds in this search are the inclusive production of V+jets, with $Z \to \nu\nu$, $W \to \ell\nu$, $Z \to \ell\ell$, and $t\bar{t}$. V+jets events are simulated at LO with MADGRAPH5_aMC@NLO v5.2.2.2 matrix element generator [42] with up to 4 partons and normalized to the next-to-next-to-leading-order (NNLO) cross section, computed using FEWZ v3.1 [43]. The V boson p_T spectra are corrected to account for next-to-leading-order (NLO) QCD and EW contributions [44]. Top quark pair ($t\bar{t}$) and single top quark in the t- and tW final states are simulated at NLO POWHEG v2 generator [45–47]. The top quark pair production is rescaled to the cross section computed with TOP++ v2.0 [48] at NNLO, and top quarks transverse momenta are corrected to match the distribution observed in data [49]. Other SM processes, such as VV and Vh production, and single top quark (t+X) production in s-channel, are simulated at NLO in QCD with MADGRAPH5_aMC@NLO using the FXFX merging scheme [50]. The minor multijet contribution is estimated through leading order samples produced with the same generator.

The hard process of all simulated samples use the NNPDF 3.0 [51] parton distribution functions (PDFs), and is interfaced with PYTHIA 8.205 [52, 53] for the parton showering and hadronization. The CUETP8M1 underlying event tune [54, 55] is used in all samples, except top quark pair production which adopts the CUETP8M2T4 tune [56].

Additional pp interactions within the same bunch crossing (pileup) are superimposed on the simulated processes, and events are weighted to match the average number (23) of interactions per bunch crossing that was observed in 2016 data taking. Generated events are processed through a full CMS detector simulation based on GEANT4 [57] and reconstructed with the same algorithms used for collision data.

4 Event reconstruction

In CMS, a global event reconstruction is performed using a particle-flow (PF) algorithm [58], which uses an optimized combination of information from the various elements of the CMS detector to identify all stable particles reconstructed in the detector as an electron, a muon, a photon, a charged hadron, or a neutral hadron.

Jets are reconstructed from PF candidates clustered using the anti-k_T algorithm [59, 60] with a distance parameter $R = 0.4$ (AK4 jets) or $R = 0.8$ (AK8 jets). Two independent algorithms are applied to mitigate the pileup effects. The AK4 and AK8 jet four-momenta are obtained by clustering candidates passing the charged hadron subtraction (CHS) algorithm [61], which discards charged hadrons not originating from the primary vertex, depending on the longitudinal impact parameter of the track. The reconstructed vertex with the largest value of summed physics-object p_T^2 is taken to be the primary pp interaction vertex. The physics objects chosen are those that have been defined using information from the tracking detector, including jets, the associated missing transverse momentum $\vec{p}_T^{\,\text{miss}}$, which was taken as the negative vector sum of the p_T of those jets, and charged leptons.

The estimated contribution of neutral particles originating from pileup interactions is estimated to be proportional to the jet area estimated using the FASTJET package [60, 62], and subtracted from the jet energy. Jet energy corrections, extracted from simulation and data in multijet, γ+jets, and Z+jets events, are applied as functions of the transverse momentum and pseudorapidity of the jet to correct the jet response and to account for residual differences between data and simulation. The jet energy resolution amounts typically to 5% at 1 TeV [63].

The mass of the AK8 jet is measured after applying the pileup per particle identification (PUPPI)

algorithm [61, 64]. The PUPPI algorithm uses a combination of the three-momenta of the particles, event pileup properties, and tracking information in order to compute a weight, assigned to charged and neutral candidates, describing the likelihood that each particle originates from a pileup interaction. The weight for charged particles not coming from the primary vertex is 0, and ranges from 0 to 1 for neutral candidates. The weight is used to rescale the particle four-momenta, superseding the need for further jet-area based pileup corrections. The PUPPI constituents are subsequently clustered with the same algorithm used for CHS AK8 jets. The soft-drop algorithm [65, 66], which is designed to remove contributions from soft radiation and additional interactions, is applied to PUPPI jets. The angular exponent parameter of the algorithm is set to $\beta = 0$, and the soft threshold to $z_{\text{cut}} = 0.1$. The soft-drop jet mass is defined as the invariant mass associated with the four-momentum of the soft-drop jet. Dedicated mass corrections, derived from simulation and data in a region enriched with $\mathrm{t\bar{t}}$ events with merged $\mathrm{W}(\mathrm{q\bar{q}})$ decays, are applied to the jet mass in order to remove residual jet p_{T} dependence [30, 67], and to match the jet mass scale and resolution observed in data. The measured soft-drop PUPPI jet mass resolution is approximately 10%. The AK8 soft drop jets are split into two subjets by reverting the last step of the clustering algorithm applied on the jet constituents.

The combined secondary vertex algorithm [68] is used for the identification of jets that originate from b quarks (b tagging), and is applied to both AK4 jets and AK8 subjets. The algorithm uses the tracks and secondary vertices associated with AK4 jets or AK8 subjets as inputs to a neural network to produce a discriminator with values between 0 and 1, with higher values indicating a higher b quark jet probability. A selection on the discriminator output is applied, corresponding to a b jet tagging efficiency of 85 or 50%, and a false-positive rate in a sample of quark and gluon jets of about 10 or 0.1%. The b tagging efficiency is corrected to take into account a difference at the percent level in algorithm performance for data and simulation [68].

Electrons are reconstructed in the fiducial region $|\eta| < 2.5$ by matching the energy deposits in the ECAL with tracks reconstructed in the tracker [69]. The electron identification is based on the distribution of energy deposited along the electron trajectory, the direction and momentum of the track, and its compatibility with the primary vertex of the event. Electrons are further required to be isolated from other energy deposits in the detector. The electron isolation parameter is defined as the sum of transverse momenta of all the PF candidates, excluding the electron itself, within $\Delta R = \sqrt{(\Delta\eta)^2 + (\Delta\phi)^2} < 0.3$ around the electron direction, where ϕ is the azimuthal angle and after the contributions from pileup and other reconstructed electrons are removed [69].

Muons are reconstructed within the acceptance of the CMS muon systems, $|\eta| < 2.4$, using the information from both the muon spectrometer and the silicon tracker [39]. Muon candidates are identified via selection criteria based on the compatibility of tracks reconstructed from silicon tracker information only with tracks reconstructed from the combination of the hits in both the tracker and muon detector. Additional requirements are based on the compatibility of the trajectory with the primary vertex, and on the number of hits observed in the tracker and muon systems. Similarly to electrons, muons are required to be isolated as well. The muon isolation is computed from reconstructed tracks within a cone $\Delta R < 0.4$ around the muon direction, ignoring the muon itself and tracks identified as originated from other muons [39].

Hadronically decaying τ leptons are reconstructed combining one or three hadronic charged PF candidates with up to two neutral pions, the latter also reconstructed by the PF algorithm from the photons arising from the $\pi^0 \to \gamma\gamma$ decay [70].

5 Event selection

Events are divided into categories depending on the number and flavor of the reconstructed charged leptons. The zero-lepton (0ℓ), the single-lepton (1ℓ) and double-lepton (2ℓ) channels are separated according to the electron and muon content in the event. These channels have different selections, aiming to maximize the V′ signal significance and the SM background discrimination. Events are further categorized depending on the number of b tagged subjets (1 or 2). In total, 10 exclusive categories are defined.

The identification criteria for the boosted Higgs boson candidate (h jet) is the same for all event categories. The highest-p_T AK8 jet in the event is required to have $p_T > 200\,\text{GeV}$ and $|\eta| < 2.5$. The soft drop jet mass m_j must fall in the interval $105 < m_j < 135\,\text{GeV}$ to enter the signal region (SR). In order to discriminate against the copious vector boson production in association with quark and gluon jets, and in order to retain the maximum signal efficiency over the whole h p_T range, the h jet is required to have 1 or 2 b tagged subjets, otherwise the event is discarded. The 2 b tagged subjet categories dominate the sensitivity at low m_X, but because of the degradation of track reconstruction at very large jet p_T, and the overlap between the two subjets of the h jet, at high m_X a significant amount of signal events is retained in the 1 b tagged subjet categories. The h jet tagging efficiency ranges between 13–24% in the 1 b tag categories, and 29–19% in the 2 b tag categories, respectively at low and high m_X. The average probability for a V+jets event to pass the h jet selections is 1.7% and 0.2% in the 1 and 2 b tag categories; the mistag rate for $\mathrm{t\bar{t}}$ events is generally larger, and corresponds to 2.9% and 0.5%, respectively.

In the 0ℓ channel, signal events are expected to have a large p_T^{miss}, defined as the magnitude of $\vec{p}_T^{\text{miss}}$, from the boosted Z boson decaying into a pair of neutrinos, which escape undetected. Data are collected using triggers that require missing hadronic activity H_T^{miss} [40] or p_T^{miss}, either with or without considering muons, larger than 90–110 GeV depending on the instantaneous luminosity. A selection is applied to the reconstructed p_T^{miss}, which is required to be larger than 250 GeV, to ensure that the trigger is fully efficient. The multijet production is suppressed by requiring that the minimum azimuthal angular separations between all AK4 and AK8 jets and the missing transverse momentum vector must satisfy $\Delta\phi(\text{jet}, \vec{p}_T^{\text{miss}}) > 0.5$. The h jet must fulfill a tighter requirement $\Delta\phi(\text{jet}, \vec{p}_T^{\text{miss}}) > 2$ and the fraction of its momentum given by the charged hadron candidates has to be larger than 0.1 to remove events arising from detector noise. Events containing isolated leptons with $p_T > 10\,\text{GeV}$, hadronically-decaying τ leptons with $p_T > 18\,\text{GeV}$ are removed in order to reduce the contribution of other SM processes. The $\mathrm{t\bar{t}}$ background contribution is reduced by removing events in which any additional AK4 jet is b tagged using an operating point 85% efficient on genuine b jets. Because of the lack of visible decay products from the Z boson, reconstruction of the resonance mass is not directly viable. Instead, the resonance mass m_X is estimated from the Higgs boson jet momentum and the $\vec{p}_T^{\text{miss}}$ which are used to compute the transverse mass $m_{\text{Vh}}^{\text{T}} = \sqrt{2 p_T^{\text{miss}} E_T^{\text{jet}} [1 - \cos\Delta\phi(\text{h jet}, \vec{p}_T^{\text{miss}})]}$.

Events in the 1e channel are collected using a trigger requiring either an isolated electron with p_T larger than 32 GeV or a non-isolated electron with p_T larger than 115 GeV. The 1μ channel requires at least one nonisolated muon with $p_T > 50\,\text{GeV}$. Moreover, the trigger criteria for the 0ℓ channel is also used for the 1ℓ channels to take advantage of the large p_T^{miss} and H_T^{miss} because of the escaping neutrino from the W decay. Offline, events are retained if exactly one lepton satisfying a p_T threshold of 55 GeV and restrictive identification and isolation criteria. The selection efficiency for the electron and the muon is approximately 75% and 95%, respectively. Simulated events are reweighted to account for small differences between data and simulation in the trigger selection, and lepton reconstruction, identification and isolation. In the 1e channel, the multijet background is further suppressed by requiring $p_T^{\text{miss}} > 80\,\text{GeV}$. Azimuthal

angular separations $\Delta\phi(\ell, \vec{p}_{\mathrm{T}}^{\,\mathrm{miss}}) < 1.5$, $\Delta\phi(\ell, \mathrm{h\,jet}) > 2$, and $\Delta\phi(\mathrm{h\,jet}, \vec{p}_{\mathrm{T}}^{\,\mathrm{miss}}) > 2$ are required to select a topology where the vector boson recoils against the Higgs boson jet. Similar to the 0ℓ selection, events with additional b tagged AK4 jets are vetoed to reduce the $\mathrm{t\bar{t}}$ background contamination. The four-momentum of the neutrino is estimated using a kinematic reconstruction technique [27]. The p_x^ν and p_y^ν components of the neutrino momentum in the transverse plane are assumed to be equal to the ones of $\vec{p}_{\mathrm{T}}^{\,\mathrm{miss}}$. By constraining the invariant mass of the sum of the charged lepton and neutrino four-momenta to be consistent with the W boson mass, a quadratic equation is derived for the longitudinal component of the neutrino momentum, p_z^ν. The reconstructed p_z^ν is chosen to be the real solution with the lower magnitude or, where both the solutions are complex, the real part with the lowest value. The sum of the neutrino and the lepton four-momenta is used to reconstruct the W boson candidate and subsequently, with the h jet four-momentum, the resonance candidate mass m_{Vh}. The former has to have a transverse momentum larger than 200 GeV and a pseudorapidity separation $|\Delta\eta(\mathrm{W,jet})| < 3$, otherwise the event is discarded.

The 2ℓ channel accepts events collected with the same triggers as in the 1ℓ channel. An additional isolated electron or muon is required to have $p_{\mathrm{T}} > 20$ GeV and the same flavor and opposite charge as the leading one. The identification and isolation requirements are looser than the 1ℓ channel, and the selection efficiency is between 85 and 90% for the electron pair, and 90 and 95% for the muon pair. The leptonic Z boson candidates require the dilepton invariant mass between 70 and 110 GeV, and a transverse momentum greater than 200 GeV. Additionally, the separation in η between the Z boson candidate and the Higgs boson jet is required to satisfy $|\Delta\eta(\mathrm{Z,jet})| < 1.3$ and $\Delta\phi(\mathrm{Z,jet}) < 2.0$ to partially reduce the dominant Z +jets background and increase the signal significance at low m_{X}, where the 2ℓ channels are more competitive. Since the $\mathrm{t\bar{t}}$ contribution is small, no veto on additional b tagged AK4 jets is applied. The resonance candidate mass m_{Vh} is defined as the invariant mass of the Z boson and the h jet.

A further requirement, applied in all channels, is to have a $m_{\mathrm{Vh}}^{\mathrm{T}}$ or m_{Vh} larger than 750 GeV, in order to ensure a sufficiently large Lorentz boost for the Higgs boson. The average signal efficiency, derived taking into account the leptonic branching fractions with respect to the leptonic decay modes of the vector bosons (ν or e, μ, and τ) and summed for the two b tag categories, is reported in Fig. 2 for the different signal models.

6 Estimated and observed background

The main background consists of a leptonically-decaying vector boson in association with jet from b or light flavor quarks, or gluons, where the light quark or gluon jets are misidentified as b jets (V+jets). A sizable background originates from the top quark events ($\mathrm{t\bar{t}}$ and t+X), whose contribution can be as large as 60% in the 1ℓ category. Minor contributions come from VV, Vh, and multijet processes. The V+jets and $\mathrm{t\bar{t}}$ backgrounds are estimated using two different procedures based on data and simulation.

The normalization of the top quark background is corrected with a scale factor determined in eight dedicated control regions, defined by inverting one selection and dropping the m_{j} requirement. In 0ℓ, 1e and 1μ categories, the veto on additional b tagged AK4 jets is inverted by requiring at least one additional AK4 jet b tagged with a tight selection to obtain a higher $\mathrm{t\bar{t}}$ purity. In the 2ℓ categories, the leptons are required to have opposite sign and different flavor (one electron and one muon), and the two leptons have to have $m_{\mathrm{e}\mu} > 110$ GeV and $p_{\mathrm{T}}^{\mathrm{e}\mu} > 120$ GeV. The scale factors are derived for each region from the ratio in event yields between data and simulation, after subtracting the contribution of the other backgrounds from

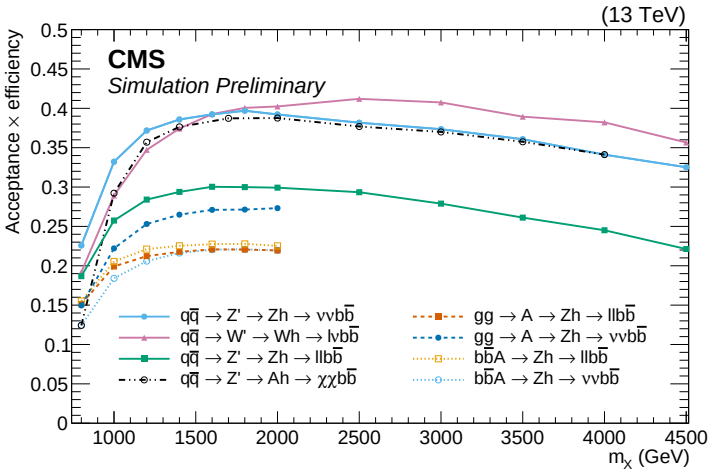

Figure 2: Event selection efficiencies for various signal processes and for different assumed masses of the resonances $m_{V'}$ or m_A. The dotted and solid lines indicate spin-0 and spin-1 resonances, respectively, in different production or decay modes. The dashed line represents the spin-1 resonance in the Z′-2HDM model with $m_A = 300\,\text{GeV}$. The efficiencies are derived by considering only the relevant decay modes of the vector bosons (electrons and muons, or τ leptons), and represent the sum of the efficiencies in the 1 and 2 b tag categories.

the data, and are applied to the corresponding signal region. The scale factors derived in the $1e, 1\mu$ top quark control regions are employed in the 2e and 2μ categories. The top quark scale factors are reported in Table 1.

Table 1: Scale factors (SF) derived to correct for the event yields of the $t\bar{t}$ and t+X backgrounds for different top quark control regions. The uncertainties because of the limited size of the data samples (stat.) and systematic effects (syst.), described in Sec. 7, are reported.

Control region		$t\bar{t}$, t+X SF $\pm$ stat. $\pm$ syst.
1 b tag	0ℓ	$1.02 \pm 0.04 \pm 0.25$
	1e	$0.91 \pm 0.02 \pm 0.25$
	1μ	$0.89 \pm 0.02 \pm 0.25$
	$1e, 1\mu$	$0.94 \pm 0.06 \pm 0.23$
2 b tag	0ℓ	$1.05 \pm 0.10 \pm 0.26$
	1e	$0.94 \pm 0.04 \pm 0.26$
	1μ	$0.85 \pm 0.03 \pm 0.26$
	$1e, 1\mu$	$1.03 \pm 0.17 \pm 0.23$

The event yields and m_{Vh} and m_{Vh}^{T} distributions of the V+jets background are determined using a procedure based on data. The background in the SR is estimated through a parametrization of the m_j distributions, considering separately V+jets, $t\bar{t}$ and t+X, and the sum of the SM diboson production processes. The m_j distributions are modeled using analytic functions, chosen based on studies in simulations, depending on the different features of the samples. The m_j spectrum in V+jets events consists of a falling distribution and is parametrized with a polynomial with 3–5 parameters depending on the signal event category. On the other hand, the m_j distribution from top quark background background has two peaks, one corresponding to a Lorentz-boosted $W \to q\bar{q}$ decay, while the other, corresponds to the top quark mass where the top quark is boosted enough for the full $t \to Wb \to q\bar{q}b$ to be merged inside the AK8 jet. The top quark mass spectrum is fixed from simulation, and the normalization is constrained from the dedicated control regions, as reported in Table 1. Diboson samples generally present peaks corresponding to the W, Z, and Higgs boson masses, and both the m_j distribution and their

event yield are taken from simulation.

The background model, built upon the sum of the V+jets, top quark, and diboson background components, is fit to the data in the two sideband regions (SB), defined as the h jet mass regions with $30 < m_{\mathrm{j}} < 65\,\mathrm{GeV}$ and $135 < m_{\mathrm{j}} < 250\,\mathrm{GeV}$, referred to as lower and higher jet mass sidebands (LSB and HSB). The mass interval $65 < m_{\mathrm{j}} < 105\,\mathrm{GeV}$ (VR), which contains vector boson merged decays, is excluded form the fit to avoid biases from a $\mathrm{X} \to \mathrm{VV}$ potential signal. In the fit, only the normalization and shape parameters of the V+jets background are free to fluctuate, and those relative to the top quark and diboson backgrounds are fixed. The expectation for each background, and the corresponding uncertainties, are determined by the integral of the fitted shapes in the SR. The procedure is repeated selecting an alternative function, consisting of the sum of an exponential and a gaussian, to model the V+jets background distribution and estimate the bias induced by the choice of the V+jets fit function. The difference between the results obtained with the nominal and the alternative function is considered as a systematic uncertainty. The expected and observed events in the SR are reported separately for each category in Table 2. The fits to the m_{j} distributions are reported in Fig. 3.

Table 2: Expected and observed numbers of events in the signal regions, for all event categories. Three separate sources of uncertainty in the expected numbers are reported: the V+jets background uncertainty from the variation of the parameters used to model the m_{j} distribution, taking into account their correlations (fit); the difference between the nominal and alternative function choice for the fit to m_{j} (alt); the $\mathrm{t\bar{t}}$, t+X uncertainties from the m_{j} modeling, the statistical component of the top quark scale factor uncertainties, and the extrapolation uncertainty from the control regions to the SR; the VV normalization uncertainties relative to the m_{j} modeling and the uncertainties affecting the normalization. A detailed description of the systematic uncertainties is provided in Sec. 7.

Category		V+jets ($\pm$fit) ($\pm$alt)	$\mathrm{t\bar{t}}$, t+X	VV	Bkg. sum	Observed
1 b tag	0ℓ	$694 \pm 17 \pm 4$	91 ± 5	34 ± 8	819 ± 20	849
	1e	$603 \pm 37 \pm 72$	700 ± 24	38 ± 10	1369 ± 85	1389
	1μ	$944 \pm 41 \pm 18$	835 ± 28	58 ± 15	1836 ± 55	1800
	2e	$71 \pm 5 \pm 5$	2 ± 1	3 ± 1	76 ± 7	68
	2μ	$78 \pm 5 \pm 5$	3 ± 1	4 ± 1	85 ± 7	95
2 b tag	0ℓ	$88 \pm 6 \pm 4$	17 ± 2	11 ± 3	116 ± 8	126
	1e	$97 \pm 8 \pm 23$	146 ± 7	7 ± 2	249 ± 25	263
	1μ	$131 \pm 9 \pm 13$	165 ± 8	10 ± 3	305 ± 18	316
	2e	$8 \pm 1 \pm 1$	1 ± 1	1 ± 1	10 ± 2	7
	2μ	$11 \pm 2 \pm 1$	1 ± 1	2 ± 1	13 ± 2	14

The m_{Vh} (or $m_{\mathrm{Vh}}^{\mathrm{T}}$) distribution of the V+jets background is derived from data in the SB, and a transfer function $\alpha(m_{\mathrm{Vh}})$ determined from simulation as:

$$\alpha(m_{\mathrm{Vh}}) = \frac{F_{\mathrm{SR}}^{\mathrm{sim,V+jets}}(m_{\mathrm{Vh}})}{F_{\mathrm{SB}}^{\mathrm{sim,V+jets}}(m_{\mathrm{Vh}})} \tag{1}$$

where $F_{\mathrm{SR}}^{\mathrm{sim,V+jets}}(m_{\mathrm{Vh}})$, $F_{\mathrm{SB}}^{\mathrm{sim,V+jets}}(m_{\mathrm{Vh}})$ represent the parametrization of the probability density functions with two-parameter exponential functions determined from the m_{Vh} spectra in the SR and the SB of the simulated V+jets sample, respectively. The $\alpha(m_{\mathrm{Vh}})$ ratio accounts for the correlations and the small kinematic differences involved in the interpolation from the sidebands to the SR, and is largely independent of the correlated uncertainties affecting the m_{Vh} shape as they cancel out in the ratio. The V+jets background prediction in the SR $F_{\mathrm{SR}}^{\mathrm{pred}}(m_{\mathrm{Vh}})$

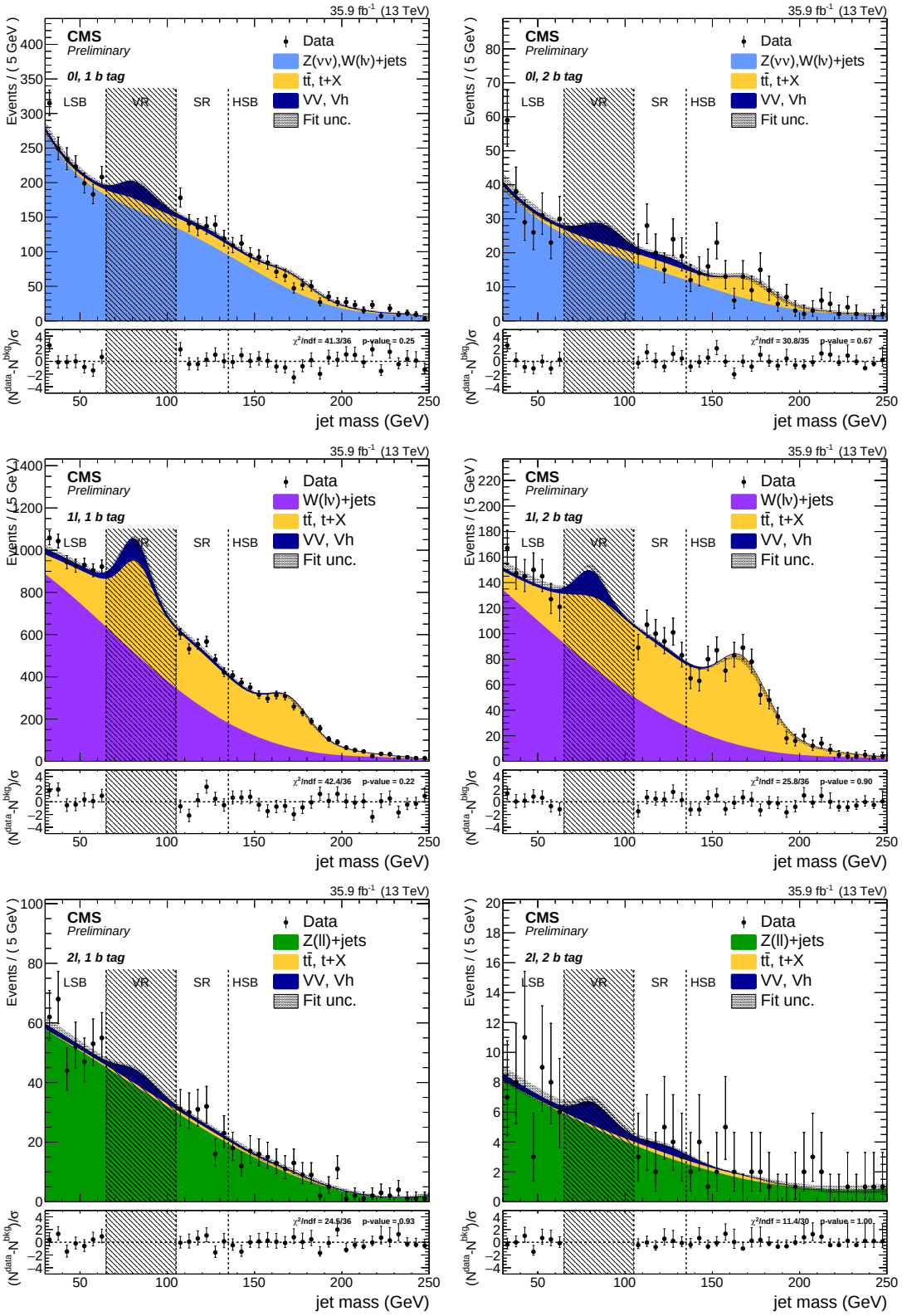

Figure 3: Soft drop PUPPI jet mass distribution of the leading AK8 jet in the 0ℓ (upper), 1ℓ (middle), and 2ℓ (lower) categories, and separately for the 1 (left) and 2 (right) b tagged subjet selections. The electron and muon categories are merged together. The shaded band represents the uncertainty from the fit to data in the jet mass sidebands. The observed data are indicated by black markers. The dashed vertical lines separate the lower (LSB) and upper (HSB) sidebands, the W and Z bosons mass region (VR), and the signal region (SR). The bottom panels report the pulls in each bin, $(N^{\text{data}} - N^{\text{bkg}})/\sigma$, where σ is the statistical uncertainty in data, as given by the Garwood interval [71].

is extracted from data in the m_{j} sidebands, after multiplying the obtained distribution by the $\alpha(m_{\mathrm{Vh}})$ ratio:

$$F_{\mathrm{SR}}^{\mathrm{pred}}(m_{\mathrm{Vh}}) = N_{\mathrm{SB}}^{\mathrm{V+jets}} F_{\mathrm{SB}}^{\mathrm{obs,V+jets}}(m_{\mathrm{Vh}})\,\alpha(m_{\mathrm{Vh}}) + N_{\mathrm{SR}}^{\mathrm{t\bar{t}}} F_{\mathrm{SR}}^{\mathrm{sim,t\bar{t}}}(m_{\mathrm{Vh}}) + N_{\mathrm{SR}}^{\mathrm{VV}} F_{\mathrm{SR}}^{\mathrm{sim,VV}}(m_{\mathrm{Vh}}) \quad (2)$$

where $F_{\mathrm{SB}}^{\mathrm{obs,V+jets}}(m_{\mathrm{Vh}})$ is the probability distribution function obtained from a fit to data in the m_{j} sidebands of the sum of the background components, and $F_{\mathrm{SR}}^{\mathrm{sim,t\bar{t}}}(m_{\mathrm{Vh}})$ and $F_{\mathrm{SR}}^{\mathrm{sim,VV}}(m_{\mathrm{Vh}})$ are the shapes of the $\mathrm{t\bar{t}}$ and diboson components, respectively. The parameters $N_{\mathrm{SB}}^{\mathrm{V+jets}}$, $N_{\mathrm{SR}}^{\mathrm{t\bar{t}}}$, $N_{\mathrm{SR}}^{\mathrm{VV}}$ are instead fixed from the fit to m_{j}, the top quark control regions, and the simulated samples, respectively. The data in the SR and the background predictions are shown in Fig. 4.

The signal mass shape is estimated from the simulated signal samples, parametrizing separately in each channel and signal hypotheses the signal distribution with a Gaussian peak and a power law to model the lower tails. The resolution of the reconstructed m_{Vh} is given by the width of the Gaussian core for the 1ℓ and 2ℓ channels and by the RMS of the $m_{\mathrm{Vh}}^{\mathrm{T}}$ distribution in the 0ℓ channel, and is found to be 10–16%, 8–5%, 5–3% of m_{X} in the 0ℓ, 1ℓ, and 2ℓ channels, respectively, when going from low to high resonance masses.

7 Systematic uncertainties

The systematic uncertainty in the V+jets and top quark background yields is dominated by the statistical uncertainty associated with the numbers of data events in the m_{j} sidebands. The uncertainties in the V+jets background shape and the secondary backgrounds are estimated from the covariance matrix of the fit to data of the m_{Vh} or $m_{\mathrm{Vh}}^{\mathrm{T}}$ distribution in the sideband regions and from the uncertainties in the modeling of the $\alpha(m_{\mathrm{Vh}})$ ratio, which depends on the numbers of data and simulation events, respectively.

The uncertainty on the top quark event yields is because of the limited number of events in the respective control regions, as reported in Table 1. The uncertainties due to the event modeling and reconstructions are not considered in the SR, because the event yield of this background is taken from data. An additional uncertainty is considered for the extrapolation from the top quark control regions to the signal region by inverting the b tag veto (3%) or changing the lepton flavor requirement (3%). Minor contributions arise from the propagation of the uncertainties in the single top and in the shape of the function modeling the m_{j} distributions of the $\mathrm{t\bar{t}}$ and VV backgrounds.

Other sources of uncertainty affect both the normalization and shape of the simulated signal and the SM diboson background. The uncertainties in the trigger efficiency and the electron, muon, and τ lepton reconstruction, identification, and isolation are evaluated through studies of events with $\mathrm{Z} \to \ell\ell$ and dilepton invariant mass around the Z boson mass, and amount to approximately 2–5% for the categories with charged leptons, and 1% in the 0ℓ categories. The jet energy scale and resolution [63] affect both shape and selection efficiencies. The jet energy corrections are also taken into account, and are responsible for a 1% variation in the numbers of background and signal events. The jet mass scale and resolution uncertainties are responsible for a 1 % and up to 6% uncertainty for the SM diboson and 11% in the signal normalization. An additional uncertainty on the shower model is evaluated with additional samples involving an Higgs boson decaying to b quark pairs showered with an alternative hadronizer are simulated with the HERWIG ++ generator [72, 73], resulting in a 6% uncertainty.

The impact on the signal efficiency because of b tagging [68] depends on the h jet p_{T} and thus on the mass of the resonance, and range from 2–5% in the 1 b tag category to 3–7% in the

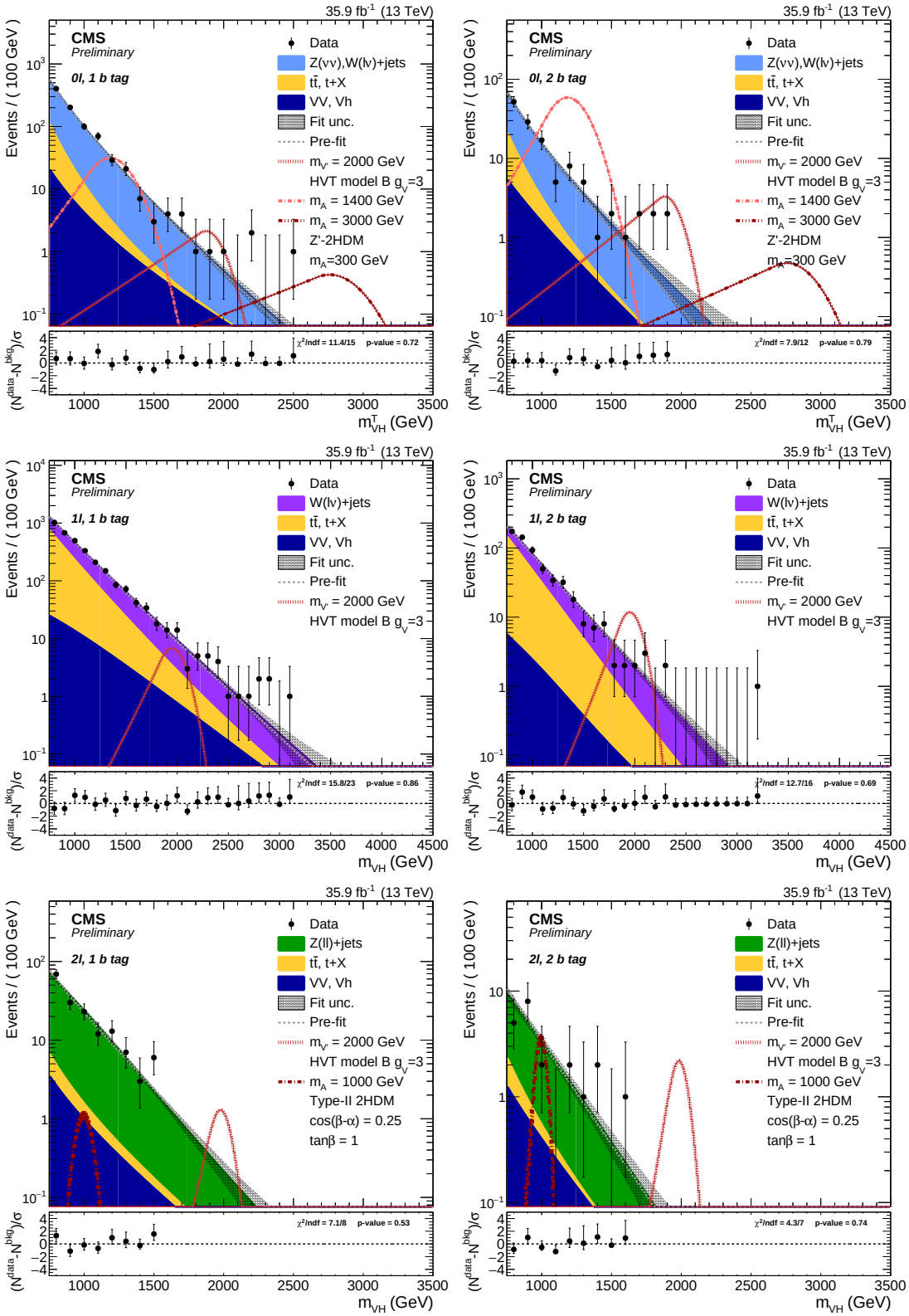

Figure 4: Resonance candidate mass m_{Vh} and transverse mass $m_{\mathrm{Vh}}^{\mathrm{T}}$ distributions in the 0ℓ (upper), 1ℓ (middle), and 2ℓ (lower) categories, and separately for the 1 (left) and 2 (right) b tagged subjet selections. Electron and muon categories are merged together. The expected background events are shown with the filled area, and the shaded band represents the total background uncertainty. The observed data are indicated by black markers, and the potential contribution of a resonance produced in the context of the HVT model B with $g_{\mathrm{V}} = 3$, or a Z'-2HDM signal with $m_{\mathrm{A}} = 300\,\mathrm{GeV}$, $m_{\chi} = 100\,\mathrm{GeV}$, and $g_{Z'} = 0.8$, are shown as dotted red lines. The bottom panels report the pulls in each bin, $(N^{\mathrm{data}} - N^{\mathrm{bkg}})/\sigma$, where σ is the statistical uncertainty in data, as given by the Garwood interval [71].

2 b tag category. The signal, VV, and t+X background event yield and selection efficiency are affected by the choice of PDFs [74] and the factorization and renormalization scale uncertainties associated with the event generators. The former are derived with SysCalc [75], and the latter are estimated by varying the corresponding scales up and down by a factor of 2. The effect of these uncertainties is approximately 21% for the $t\bar{t}$ background, and can be as large as 30% depending on the signal resonance mass. The top quark background is also affected by the uncertainty on the p_T spectrum [49], which accounts for up to 14% uncertainty propagated to the top quark scale factors. Additional systematic uncertainties affecting the event yield of backgrounds and signal from pileup contributions, integrated luminosity [76], the impact of jet energy scale and resolution on p_T^{miss} are also included in the analysis. A summary of the systematic uncertainties is reported in Table 3.

Table 3: Summary of systematic uncertainties for the backgrounds and signal samples. The entries labeled with § are also propagated to the shapes of the distributions. Uncertainties marked with † only affect the top quark scale factors. The uncertainties marked with ‡ have impact on the signal cross section.

	V+jets	$t\bar{t}$, t+X	VV	Signal
bkg. normalization	2–15%	-	-	-
top scale factors	-	2–17%	-	-
jet energy scale §	-	-	3%	1%
jet energy resolution §	-	-	<1%	<1%
jet mass scale	-	-	6%	1%
jet mass resolution	-	-	6%	11%
lepton identification and isolation	-	1–3% †	2–4% (e), 4–5% (μ), 1% (0ℓ)	
lepton scale and res. §	-	-	-	1–5%
τ veto	-	-	3% (0ℓ)	
p_T^{miss} scale and res.	-	-	1%	1%
trigger	-	-	4% (e), 4% (μ), 3% (0ℓ)	
b tagging	-	3% (0ℓ, 1ℓ) 2–5% †	4% (1b) 5% (2b)	2–5% (1b) 3–7% (2b)
Higgs boson jet	-	-	-	6%
top quark p_T	-	6–14% †	-	-
pileup	-	<1% †	<1%	<1%
factorization and renormalization scales	-	21% †	19%	3–28% ‡
PDF normalization	-	5% †	5%	8–36% ‡
PDF acceptance	-	2% †	<2%	<1%
luminosity	-	-	2.5%	2.5%

8 Results and interpretation

Results are obtained from a combined signal and background fit to the unbinned m_{Vh} or m_{Vh}^T distribution, based on a profile likelihood. Systematic uncertainties are treated as nuisance parameters and are profiled in the statistical interpretation [77–79]. The background-only hypothesis is tested against the $X \to Vh$ signal in the ten categories. The asymptotic modified frequentist method [80] is used to determine limits at 95% confidence level (CL) on the contribution from signal. Limits are derived on the product of the cross section for a heavy boson X and the branching fractions for the decays $X \to Vh$ and $h \to b\bar{b}$, denoted $\sigma(X)\,\mathcal{B}(X \to Vh)\,\mathcal{B}(h \to b\bar{b})$.

The 0ℓ and 2ℓ categories are combined to provide upper limits for the case where X is a heavy spin-1 vector singlet Z′ or a pseudoscalar boson A; similarly, the 1ℓ categories are combined to provide limits for the case where X is a heavy W′. The 0ℓ categories are also used to place limits on the Z′-2HDM model. The uncertainties on the signal cross section (marked with ‡ in Table 3) are not profiled in the fit when presenting the results as upper limits on the cross sections, and are reported on the theory line as uncertainty band. On the other hand, when placing constraints on the model parameters, the uncertainties are profiled in the fit.

The exclusion limits for spin-1 singlet hypotheses (Z′ or W′) are reported in Fig. 5. The HVT triplet hypothesis is tested by combining the 0ℓ, 1ℓ, and 2ℓ categories and adding the Z′ and W′ cross sections in Fig. 6, and taking into account the event migrations between categories in the signal if leptons do not pass the acceptance or analysis requirements. The predictions of the HVT models A and B are superimposed on the exclusion limits, and a heavy triplet with $m_{V'} < 2.8$ and 2.9 TeV is excluded at 95% CL in the HVT model A and B, respectively. These results are similar to those reported in the ATLAS search performed on the same final states and a comparable dataset [28].

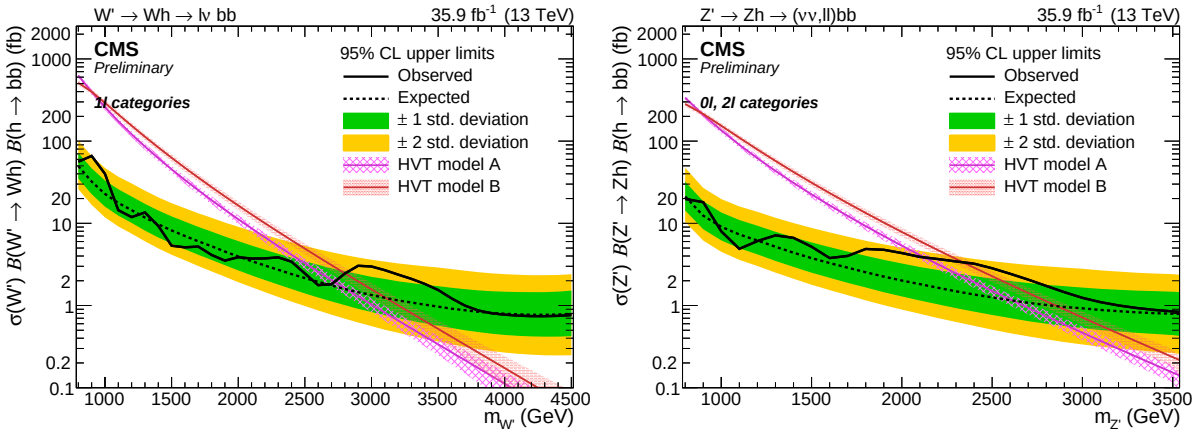

Figure 5: Observed and expected 95% CL upper limits on $\sigma(W')\,\mathcal{B}(W' \to Wh)\,\mathcal{B}(h \to b\bar{b})$ (left) and $\sigma(Z')\,\mathcal{B}(Z' \to Zh)\,\mathcal{B}(h \to b\bar{b})$ (right) for various mass hypotheses of a single narrow spin-1 resonance. The inner green and outer yellow bands represent the ± 1 and ± 2 standard deviation (std.) variation on the expected limits. The solid curves and their shaded areas correspond to the product of the cross sections and the branching fractions predicted by the HVT model A and B and the relative uncertainties.

The exclusion limits on the resonance cross section shown in Fig. 6 can be interpreted as a limit in the $[g_V c_H,\ g^2 c_F / g_V]$ plane of the HVT parameters. The excluded region of the parameter space for narrow resonances relative to the combination of all the considered channels is shown in Fig. 7. The fraction of the parameter space where the natural width of the resonances is larger than the average experimental resolution of 4%, and thus the narrow width approximation is not valid, is also indicated in Fig. 7. The exclusion of the parameter space significantly improves on the reach of the previous $\sqrt{s} = 13$ TeV and $\sqrt{s} = 8$ TeV searches in the same final states [27, 28, 33].

Figure 8 reports the exclusion limits as a function of the A boson mass on the products of the A boson cross sections in the two considered production processes, the gluon-gluon fusion and b quark associated production, and the branching fractions $\mathcal{B}(A \to Zh)$ and $\mathcal{B}(h \to b\bar{b})$. The 2HDM cross sections and branching fractions are computed at NNLO with 2HDMC 1.7.0 [81] and SUSHI 1.6.1 [82], respectively. The parameters used for the models are: $m_h = 125$ GeV, $m_H = m_{H^\pm} = m_A$, $m_{12}^2 = m_A^2 \frac{\tan\beta}{1+\tan^2\beta}$ to break the discrete Z_2 symmetry as in the MSSM, and

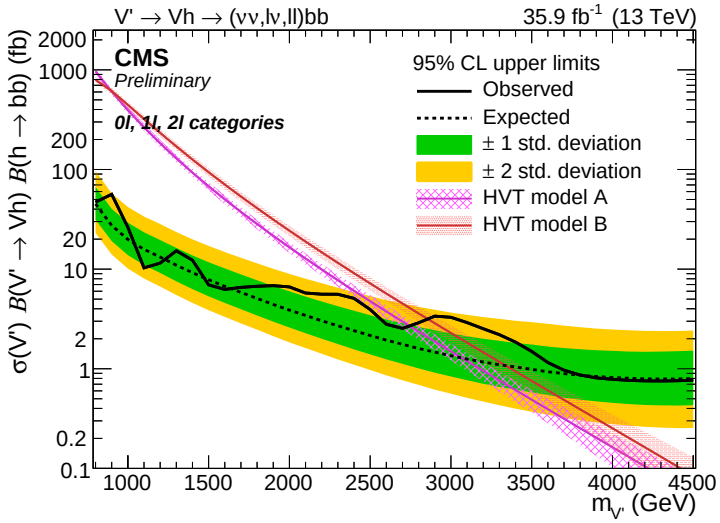

Figure 6: Observed and expected 95% CL upper limit with the ± 1 and ± 2 standard deviation uncertainty bands on $\sigma(\mathrm{X})\,\mathcal{B}(\mathrm{X} \to \mathrm{Vh})\,\mathcal{B}(\mathrm{h} \to \mathrm{b\bar{b}})$ as a function of the HVT triplet mass, for the combination of all the considered channels. The solid curves and their shaded areas correspond to the cross sections predicted by the HVT model A and B and the relative uncertainties.

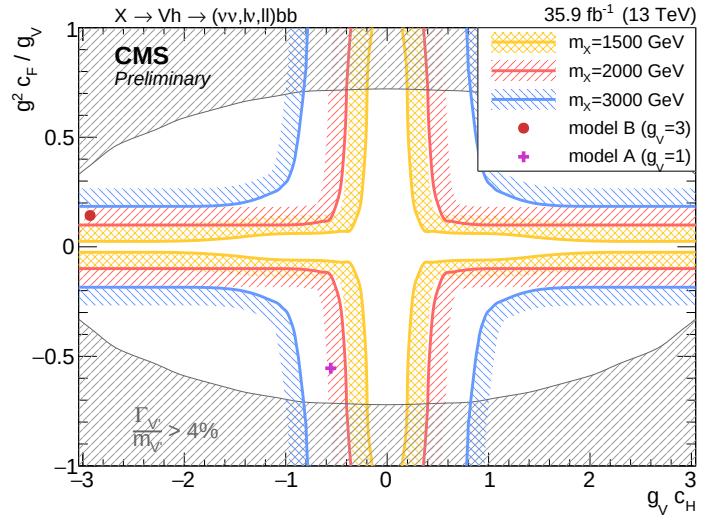

Figure 7: Observed exclusion limits in the HVT parameter plane $[g_{\mathrm{V}}c_{\mathrm{H}},\, g^2 c_{\mathrm{F}}/g_{\mathrm{V}}]$ for three different resonance masses (1.5, 2.0, and 3.0 TeV). The benchmark scenarios corresponding to HVT model A and model B are represented by a purple cross and a red point. The gray shaded area corresponds to the region where the resonance natural width ($\Gamma_{\mathrm{V}'}$) is predicted to be larger than the typical experimental resolution (4%), and thus the narrow-width approximation is not fulfilled.

$\lambda_{6,7} = 0$ to ensure CP conservation at tree level in the 2HDM Higgs sector [20]. In the scenario with $\cos(\beta - \alpha) = 0.25$ and $\tan\beta = 1$, an A boson up to 1150 GeV and 1230 GeV is excluded in 2HDM Type-I and Type-II, respectively. These exclusion limits are used to place constraints on the two-dimensional plane of the 2HDM parameters $[\cos(\beta - \alpha), \tan\beta]$ as reported in Fig. 9, with fixed $m_{\mathrm{A}} = 1000$ GeV in the range $0.1 \leq \tan\beta \leq 100$ and $-1 \leq \cos(\beta - \alpha) \leq 1$, using the convention $0 < \beta - \alpha < \pi$. These results extend the search for a 2HDM pseudoscalar boson A up to 2 TeV, which is a kinematic region previously unexplored by CMS in the Run I search [32], and provide comparable limits to the ATLAS search [28].

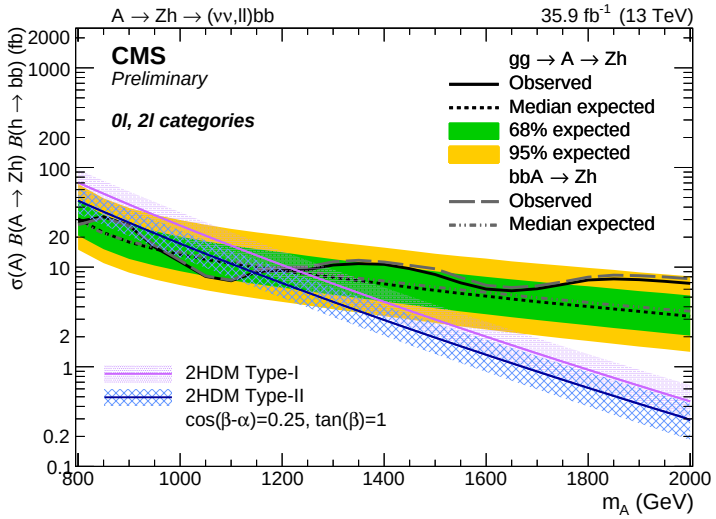

Figure 8: Observed and expected 95% CL upper limit with the ± 1 and ± 2 standard deviation bands on $\sigma(\mathrm{A})\,\mathcal{B}(\mathrm{A} \to \mathrm{Zh})\,\mathcal{B}(\mathrm{h} \to \mathrm{b\bar{b}})$ as a function of m_A for the combination of the 0ℓ and 2ℓ channels. The solid line represent the exclusion for a spin-0 signal produced through gluon-gluon fusion, and dashed line represent the b quark associated production. The solid lines and their shaded area represent the corresponding values predicted by the Type-I and Type-II 2HDM model fixing the parameters $\cos(\beta - \alpha) = 0.25$ and $\tan\beta = 1$ parameters. In this scenario, the b quark associated production is negligible, and the A is predominantly produced through gluon-gluon fusion.

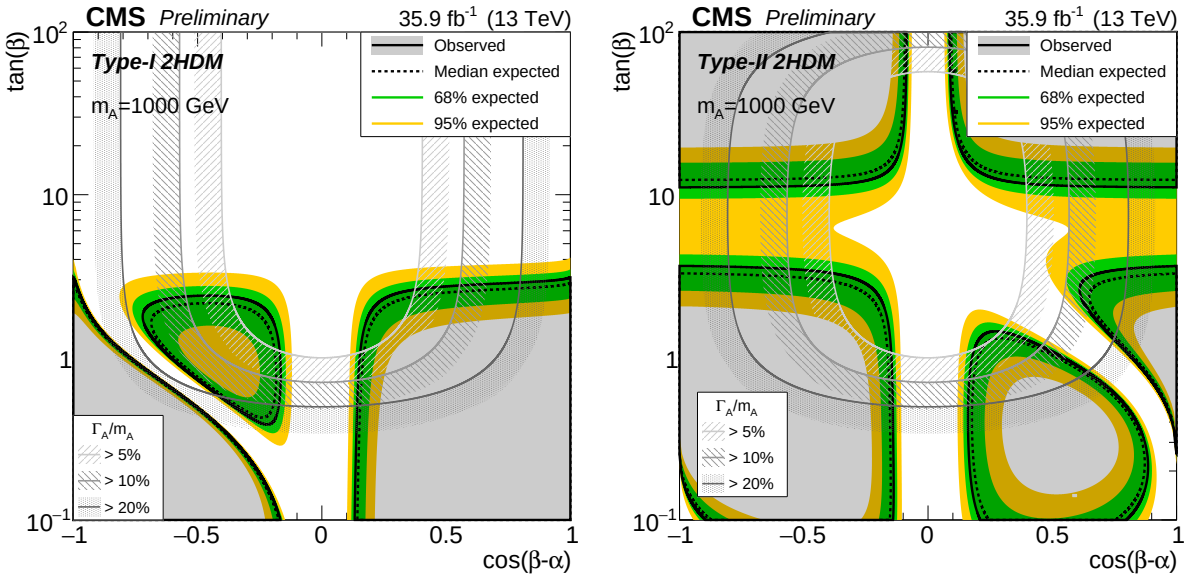

Figure 9: Observed and expected exclusion limit for Type-I (left) and Type-II 2HDM models (right) in the [$\tan\beta$, $\cos(\beta - \alpha)$] plane and assuming a fixed $m_\mathrm{A} = 1\,\mathrm{TeV}$. The light shaded areas identify regions with different resonance natural width (5%, 10%, 20% of the resonance mass).

The exclusion of the parameter space of the Z′-2HDM model is presented in Fig. 10 in the considered benchmark point with $g_{Z'} = 0.8$, $g_\chi = 1$, $m_\chi = 100\,\mathrm{GeV}$, and $\tan\beta = 1$. The branching fraction of the A boson decaying to DM particles accounts for other decay channels as predicted by the Z′-2HDM model, and SM branching fractions are assumed for the

Higgs boson [41]. The exclusion limits are presented as an exclusion of the $m_{Z'}$ and m_A parameter space in Fig. 10. With the current dataset, $m_{Z'}$ up to 3.2 TeV and m_A up to 800 GeV are excluded, providing a more sensitive result compared to the ATLAS search performed on a similar dataset [35], which excluded a $m_{Z'} < 2.5$ TeV and $m_A < 600$ GeV, and setting the most stringent constrain to date on the Z′-2HDM model.

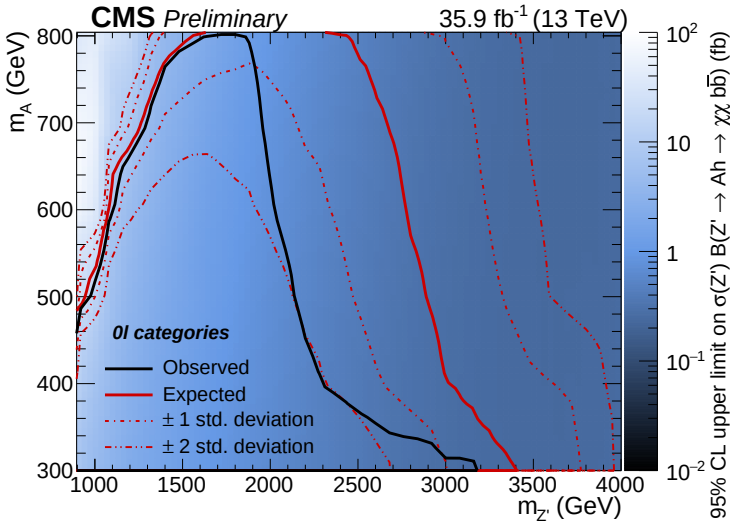

Figure 10: Observed and expected exclusion on the parameter plane $[m_{Z'}, m_A]$. The excluded region in the considered benchmark scenario ($g_{Z'} = 0.8$, $g_\chi = 1$, $\tan\beta = 1$, $m_\chi = 100$ GeV, and $m_A = m_H = m_{H^\pm}$) is represented by the shaded area.

9 Summary

A search for a resonance with mass between 800 and 4500 GeV, decaying to a standard model (SM) vector boson and a SM Higgs boson, is reported. The data sample was collected by the CMS experiment at $\sqrt{s} = 13$ TeV, and corresponds to an integrated luminosity of 35.9 fb^{-1}. The final states contained the leptonic decays of the vector bosons, in events with zero, exactly one, and two electrons or muons. The standard model Higgs boson is reconstructed from its decay to b quark-antiquark pairs. Depending on the resonance mass, upper limits in the range 0.8–60 fb are set on the product of the cross sections and the branching fractions for the decay of the resonance into a Higgs and a vector boson, and for the decay of the Higgs boson into a pair of b quarks. In a triplet of narrow spin-1 resonances, vector bosons with a mass lower than 2.8 and 2.9 TeV are excluded in the benchmark scenarios A and B, respectively. Furthermore, the results of this search provide an exclusion in the two Higgs doublet model (2HDM) parameter space up to 2 TeV, which is a kinematic region previously unexplored by previous CMS searches, and a heavy pseudoscalar boson with mass lower than 1.1 TeV and 1.2 TeV is excluded in the $\cos(\beta - \alpha) = 0.25$ and $\tan\beta = 1$ scenario. A significant reduction of the allowed parameter space is also placed on the Z′-2HDM model that includes a dark matter candidate, excluding a Z′ boson mass up to 3.2 TeV, and a pseudoscalar boson A up to 800 GeV in the considered benchmark scenario, placing the most stringent limits on this model to date.

Acknowledgments

We congratulate our colleagues in the CERN accelerator departments for the excellent performance of the LHC and thank the technical and administrative staffs at CERN and at other CMS

institutes for their contributions to the success of the CMS effort. In addition, we gratefully acknowledge the computing centers and personnel of the Worldwide LHC Computing Grid for delivering so effectively the computing infrastructure essential to our analyses. Finally, we acknowledge the enduring support for the construction and operation of the LHC and the CMS detector provided by the following funding agencies: BMWFW and FWF (Austria); FNRS and FWO (Belgium); CNPq, CAPES, FAPERJ, and FAPESP (Brazil); MES (Bulgaria); CERN; CAS, MoST, and NSFC (China); COLCIENCIAS (Colombia); MSES and CSF (Croatia); RPF (Cyprus); SENESCYT (Ecuador); MoER, ERC IUT, and ERDF (Estonia); Academy of Finland, MEC, and HIP (Finland); CEA and CNRS/IN2P3 (France); BMBF, DFG, and HGF (Germany); GSRT (Greece); OTKA and NIH (Hungary); DAE and DST (India); IPM (Iran); SFI (Ireland); INFN (Italy); MSIP and NRF (Republic of Korea); LAS (Lithuania); MOE and UM (Malaysia); BUAP, CINVESTAV, CONACYT, LNS, SEP, and UASLP-FAI (Mexico); MBIE (New Zealand); PAEC (Pakistan); MSHE and NSC (Poland); FCT (Portugal); JINR (Dubna); MON, RosAtom, RAS, and RFBR (Russia); MESTD (Serbia); SEIDI and CPAN (Spain); Swiss Funding Agencies (Switzerland); MST (Taipei); ThEPCenter, IPST, STAR, and NSTDA (Thailand); TUBITAK and TAEK (Turkey); NASU and SFFR (Ukraine); STFC (United Kingdom); DOE and NSF (USA).

Individuals have received support from the Marie-Curie program and the European Research Council and EPLANET (European Union); the Leventis Foundation; the A. P. Sloan Foundation; the Alexander von Humboldt Foundation; the Belgian Federal Science Policy Office; the Fonds pour la Formation à la Recherche dans l'Industrie et dans l'Agriculture (FRIA-Belgium); the Agentschap voor Innovatie door Wetenschap en Technologie (IWT-Belgium); the Ministry of Education, Youth and Sports (MEYS) of the Czech Republic; the Council of Science and Industrial Research, India; the HOMING PLUS program of the Foundation for Polish Science, cofinanced from European Union, Regional Development Fund, the Mobility Plus program of the Ministry of Science and Higher Education, the National Science Center (Poland), contracts Harmonia 2014/14/M/ST2/00428, Opus 2013/11/B/ST2/04202, 2014/13/B/ST2/02543 and 2014/15/B/ST2/03998, Sonata-bis 2012/07/E/ST2/01406; the Thalis and Aristeia programs cofinanced by EU-ESF and the Greek NSRF; the National Priorities Research Program by Qatar National Research Fund; the Programa Clarín-COFUND del Principado de Asturias; the Rachadapisek Sompot Fund for Postdoctoral Fellowship, Chulalongkorn University and the Chulalongkorn Academic into Its 2nd Century Project Advancement Project (Thailand); and the Welch Foundation, contract C-1845.

References

[1] ATLAS Collaboration, "Observation of a new particle in the search for the Standard Model Higgs boson with the ATLAS detector at the LHC", *Phys. Lett. B* **716** (2012) 1, doi:10.1016/j.physletb.2012.08.020, arXiv:1207.7214.

[2] CMS Collaboration, "Observation of a new boson at a mass of 125 GeV with the CMS experiment at the LHC", *Phys. Lett. B* **716** (2012) 30, doi:10.1016/j.physletb.2012.08.021, arXiv:1207.7235.

[3] CMS Collaboration, "Observation of a new boson with mass near 125 GeV in pp collisions at $\sqrt{s}$ = 7 and 8 TeV", *JHEP* **06** (2013) 081, doi:10.1007/JHEP06(2013)081, arXiv:1303.4571.

[4] ATLAS Collaboration, "Measurement of the Higgs boson mass from the $H \to \gamma\gamma$ and $H \to ZZ^* \to 4\ell$ channels in pp collisions at center-of-mass energies of 7 and 8 TeV with

the ATLAS detector", *Phys. Rev. D* **90** (2014) 052004, doi:10.1103/PhysRevD.90.052004, arXiv:1406.3827.

[5] CMS Collaboration, "Precise determination of the mass of the Higgs boson and tests of compatibility of its couplings with the standard model predictions using proton collisions at 7 and 8 TeV", *Eur. Phys. J. C* **75** (2015) 212, doi:10.1140/epjc/s10052-015-3351-7, arXiv:1412.8662.

[6] CMS Collaboration, "Evidence for the direct decay of the 125 GeV Higgs boson to fermions", *Nature Phys.* **10** (2014) 557, doi:10.1038/nphys3005, arXiv:1401.6527.

[7] ATLAS and CMS Collaborations, "Combined measurement of the Higgs boson mass in pp collisions at $\sqrt{s} = 7$ and 8 TeV with the ATLAS and CMS experiments", *Phys. Rev. Lett.* **114** (2015) 191803, doi:10.1103/PhysRevLett.114.191803, arXiv:1503.07589.

[8] G. F. Giudice, "Naturally Speaking: The Naturalness Criterion and Physics at the LHC", doi:10.1142/9789812779762_0010, arXiv:0801.2562. To be published in the book "LHC Perspectives", edited by G. Kane and A. Pierce.

[9] C. Grojean, E. Salvioni, and R. Torre, "A weakly constrained W′ at the early LHC", *JHEP* **07** (2011) 002, doi:10.1007/JHEP07(2011)002, arXiv:1103.2761.

[10] V. D. Barger, W.-Y. Keung, and E. Ma, "A gauge model with light W and Z bosons", *Phys. Rev. D* **22** (1980) 727, doi:10.1103/PhysRevD.22.727.

[11] E. Salvioni, G. Villadoro, and F. Zwirner, "Minimal Z' models: present bounds and early LHC reach", *JHEP* **09** (2009) 068, doi:10.1088/1126-6708/2009/11/068, arXiv:0909.1320.

[12] R. Contino, D. Pappadopulo, D. Marzocca, and R. Rattazzi, "On the effect of resonances in composite Higgs phenomenology", *JHEP* **10** (2011) 081, doi:10.1007/JHEP10(2011)081, arXiv:1109.1570.

[13] D. Marzocca, M. Serone, and J. Shu, "General composite Higgs models", *JHEP* **08** (2012) 13, doi:10.1007/JHEP08(2012)013, arXiv:1205.0770.

[14] B. Bellazzini, C. Csaki, and J. Serra, "Composite Higgses", *Eur. Phys. J. C* **74** (2014) 2766, doi:10.1140/epjc/s10052-014-2766-x, arXiv:1401.2457.

[15] K. Lane and L. Pritchett, "The light composite Higgs boson in strong extended technicolor", *JHEP* **06** (2017) 140, doi:10.1007/JHEP06(2017)140, arXiv:1604.07085.

[16] T. Han, H. E. Logan, B. McElrath, and L.-T. Wang, "Phenomenology of the little Higgs model", *Phys. Rev. D* **67** (2003) 095004, doi:10.1103/PhysRevD.67.095004, arXiv:hep-ph/0301040.

[17] M. Schmaltz and D. Tucker-Smith, "Little Higgs theories", *Ann. Rev. Nucl. Part. Sci.* **55** (2005) 229, doi:10.1146/annurev.nucl.55.090704.151502, arXiv:hep-ph/0502182.

[18] M. Perelstein, "Little Higgs models and their phenomenology", *Prog. Part. Nucl. Phys.* **58** (2007) 247, doi:10.1016/j.ppnp.2006.04.001, arXiv:hep-ph/0512128.

[19] D. Pappadopulo, A. Thamm, R. Torre, and A. Wulzer, "Heavy vector triplets: bridging theory and data", *JHEP* **09** (2014) 60, doi:10.1007/JHEP09(2014)060, arXiv:1402.4431.

[20] G. C. Branco et al., "Theory and phenomenology of two-Higgs-doublet models", *Phys. Rep.* **516** (2012) 1, doi:10.1016/j.physrep.2012.02.002, arXiv:1106.0034.

[21] A. Berlin, T. Lin, and L.-T. Wang, "Mono-Higgs Detection of Dark Matter at the LHC", *JHEP* **06** (2014) 078, doi:10.1007/JHEP06(2014)078, arXiv:1402.7074.

[22] L. Carpenter et al., "Mono-Higgs-boson: A new collider probe of dark matter", *Phys. Rev. D* **89** (2014) 075017, doi:10.1103/PhysRevD.89.075017, arXiv:1312.2592.

[23] ATLAS Collaboration, "Search for a new resonance decaying to a W or Z boson and a Higgs boson in the $\ell\ell/\ell\nu/\nu\nu + b\bar{b}$ final states with the ATLAS detector", *Eur. Phys. J. C* **75** (2015) 263, doi:10.1140/epjc/s10052-015-3474-x, arXiv:1503.08089.

[24] CMS Collaboration, "Search for narrow high-mass resonances in proton-proton collisions at $\sqrt{s}$ = 8 TeV decaying to a Z and a Higgs boson", *Phys. Lett. B* **748** (2015) 255, doi:10.1016/j.physletb.2015.07.011, arXiv:1502.04994.

[25] CMS Collaboration, "Search for massive resonances decaying into WW, WZ, ZZ, qW, and qZ with dijet final states at sqrt(s) = 13 TeV", arXiv:1708.05379. Submitted to *Phys. Rev. D*.

[26] ATLAS Collaboration, "Searches for heavy diboson resonances in pp collisions at $\sqrt{s} = 13$ TeV with the ATLAS detector", *JHEP* **09** (2016) 173, doi:10.1007/JHEP09(2016)173, arXiv:1606.04833.

[27] CMS Collaboration, "Search for heavy resonances decaying into a vector boson and a Higgs boson in final states with charged leptons, neutrinos, and b quarks", *Phys. Lett. B* **768** (2017) 137, doi:10.1016/j.physletb.2017.02.040, arXiv:1610.08066.

[28] ATLAS Collaboration, "Search for heavy resonances decaying into a W or Z boson and a Higgs boson in final states with leptons and b-jets in 36 fb^{-1} of $\sqrt{s} = 13$ TeV pp collisions with the ATLAS detector", arXiv:1712.06518. Submitted to JHEP.

[29] ATLAS Collaboration, "Search for new resonances decaying to a W or Z boson and a Higgs boson in the $\ell^+\ell^- b\bar{b}$, $\ell\nu b\bar{b}$, and $\nu\bar{\nu}b\bar{b}$ channels with pp collisions at $\sqrt{s} = 13$ TeV with the ATLAS detector", *Phys. Lett. B* **765** (2016) 32, doi:10.1016/j.physletb.2016.11.045, arXiv:1607.05621.

[30] CMS Collaboration, "Search for heavy resonances that decay into a vector boson and a Higgs boson in hadronic final states at $\sqrt{s} = 13$ TeV", *Eur. Phys. J. C* **77** (2017) 636, doi:10.1140/epjc/s10052-017-5192-z, arXiv:1707.01303.

[31] ATLAS Collaboration, "Search for heavy resonances decaying to a W or Z boson and a Higgs boson in the $q\bar{q}^{(\prime)}b\bar{b}$ final state in pp collisions at $\sqrt{s} = 13$ TeV with the ATLAS detector", arXiv:1707.06958. Submitted to *Phys. Lett. B*.

[32] CMS Collaboration, "Search for a pseudoscalar boson decaying into a Z boson and the 125 GeV Higgs boson in $\ell^+\ell^- b\bar{b}$ final states", *Phys. Lett. B* **748** (2015) 221, doi:10.1016/j.physletb.2015.07.010, arXiv:1504.04710.

[33] CMS Collaboration, "Search for massive WH resonances decaying into the $\ell\nu b\bar{b}$ final state at $\sqrt{s} = 8$ TeV", *Eur. Phys. J. C* **76** (2016) 1, doi:10.1140/epjc/s10052-016-4067-z, arXiv:1601.06431.

[34] CMS Collaboration, "Search for associated production of dark matter with a Higgs boson decaying to $b\bar{b}$ or $\gamma\gamma$ at $\sqrt{s}$ = 13 TeV", arXiv:1703.05236. Submitted to *JHEP*.

[35] ATLAS Collaboration, "Search for Dark Matter Produced in Association with a Higgs Boson Decaying to $b\bar{b}$ using 36 fb^{-1} of pp collisions at $\sqrt{s} = 13$ TeV with the ATLAS Detector", *Phys. Rev. Lett.* **119** (2017) 181804, doi:10.1103/PhysRevLett.119.181804, arXiv:1707.01302.

[36] LHC Higgs Cross Section Working Group, "Handbook of LHC Higgs Cross Sections: 3. Higgs Properties", *CERN-2013-004* (2013) doi:10.5170/CERN-2013-004, arXiv:1307.1347.

[37] CMS Collaboration, "The CMS experiment at the CERN LHC", *JINST* **3** (2008) S08004, doi:10.1088/1748-0221/3/08/S08004.

[38] CMS Collaboration, "Description and performance of track and primary-vertex reconstruction with the CMS tracker", *JINST* **9** (2014) P10009, doi:10.1088/1748-0221/9/10/P10009, arXiv:1405.6569.

[39] CMS Collaboration, "Performance of CMS muon reconstruction in pp collision events at $\sqrt{s} = 7$ TeV", *JINST* **7** (2012) P10002, doi:10.1088/1748-0221/7/10/P10002, arXiv:1206.4071.

[40] CMS Collaboration, "The CMS trigger system", *JINST* **12** (2017) P01020, doi:10.1088/1748-0221/12/01/P01020, arXiv:1609.02366.

[41] D. Abercrombie et al., "Dark Matter Benchmark Models for Early LHC Run-2 Searches: Report of the ATLAS/CMS Dark Matter Forum", arXiv:1507.00966.

[42] J. Alwall et al., "The automated computation of tree-level and next-to-leading order differential cross sections, and their matching to parton shower simulations", *JHEP* **07** (2014) 079, doi:10.1007/JHEP07(2014)079, arXiv:1405.0301.

[43] Y. Li and F. Petriello, "Combining QCD and electroweak corrections to dilepton production in FEWZ", *Phys. Rev. D* **86** (2012) 094034, doi:10.1103/PhysRevD.86.094034, arXiv:1208.5967.

[44] S. Kallweit et al., "NLO QCD+EW predictions for V+jets including off-shell vector-boson decays and multijet merging", *JHEP* **04** (2016) 021, doi:10.1007/JHEP04(2016)021, arXiv:1511.08692.

[45] P. Nason, "A new method for combining NLO QCD with shower Monte Carlo algorithms", *JHEP* **11** (2004) 040, doi:10.1088/1126-6708/2004/11/040, arXiv:hep-ph/0409146.

[46] S. Frixione, P. Nason, and C. Oleari, "Matching NLO QCD computations with Parton Shower simulations: the POWHEG method", *JHEP* **11** (2007) 070, doi:10.1088/1126-6708/2007/11/070, arXiv:0709.2092.

[47] S. Alioli, P. Nason, C. Oleari, and E. Re, "A general framework for implementing NLO calculations in shower Monte Carlo programs: the POWHEG BOX", *JHEP* **06** (2010) 043, doi:10.1007/JHEP06(2010)043, arXiv:1002.2581.

[48] M. Czakon and A. Mitov, "Top++: A program for the calculation of the top-pair cross-section at hadron colliders", *Comput. Phys. Commun.* **185** (2014) 2930, doi:10.1016/j.cpc.2014.06.021, arXiv:1112.5675.

[49] CMS Collaboration, "Measurement of differential cross sections for top quark pair production using the lepton+jets final state in proton-proton collisions at 13 TeV", *Phys. Rev. D* **95** (2017) 092001, doi:10.1103/PhysRevD.95.092001, arXiv:1610.04191.

[50] R. Frederix and S. Frixione, "Merging meets matching in MC@NLO", *JHEP* **12** (2012) 061, doi:10.1007/JHEP12(2012)061, arXiv:1209.6215.

[51] NNPDF Collaboration, "Parton distributions for the LHC Run II", *JHEP* **04** (2015) 040, doi:10.1007/JHEP04(2015)040, arXiv:1410.8849.

[52] T. Sjöstrand, S. Mrenna, and P. Skands, "A brief introduction to PYTHIA 8.1", *Comput. Phys. Commun.* **178** (2008) 852, doi:10.1016/j.cpc.2008.01.036, arXiv:0710.3820.

[53] T. Sjöstrand, S. Mrenna, and P. Skands, "PYTHIA 6.4 physics and manual", *JHEP* **05** (2006) 026, doi:10.1088/1126-6708/2006/05/026, arXiv:hep-ph/0603175.

[54] P. Skands, S. Carrazza, and J. Rojo, "Tuning PYTHIA 8.1: the Monash 2013 Tune", *Eur. Phys. J. C* **74** (2014) 3024, doi:10.1140/epjc/s10052-014-3024-y, arXiv:1404.5630.

[55] CMS Collaboration, "Event generator tunes obtained from underlying event and multiparton scattering measurements", *Eur. Phys. J. C* **76** (2016) 155, doi:10.1140/epjc/s10052-016-3988-x, arXiv:1512.00815.

[56] CMS Collaboration, "Investigations of the impact of the parton shower tuning in Pythia 8 in the modelling of $\mathrm{t\bar{t}}$ at $\sqrt{s} = 8$ and 13 TeV", CMS Physics Analysis Summary CMS-PAS-TOP-16-021, CERN, 2016.

[57] GEANT4 Collaboration, "GEANT4—a simulation toolkit", *Nucl. Instrum. Meth. A* **506** (2003) 250, doi:10.1016/S0168-9002(03)01368-8.

[58] CMS Collaboration, "Particle-flow reconstruction and global event description with the cms detector", *JINST* **12** (2017) P10003, doi:10.1088/1748-0221/12/10/P10003, arXiv:1706.04965.

[59] M. Cacciari, G. P. Salam, and G. Soyez, "The anti-k_t jet clustering algorithm", *JHEP* **04** (2008) 063, doi:10.1088/1126-6708/2008/04/063, arXiv:0802.1189.

[60] M. Cacciari, G. P. Salam, and G. Soyez, "FastJet user manual", *Eur. Phys. J. C* **72** (2012) 1896, doi:10.1140/epjc/s10052-012-1896-2, arXiv:1111.6097.

[61] CMS Collaboration, "Pileup removal algorithms", CMS Physics Analysis Summary CMS-PAS-JME-14-001, CERN, 2014.

[62] M. Cacciari, G. P. Salam, and G. Soyez, "The catchment area of jets", *JHEP* **04** (2008) 005, doi:10.1088/1126-6708/2008/04/005, arXiv:0802.1188.

[63] CMS Collaboration, "Jet energy scale and resolution in the CMS experiment in pp collisions at 8 TeV", *JINST* **12** (2017) P02014, doi:10.1088/1748-0221/12/02/P02014, arXiv:1607.03663.

[64] D. Bertolini, P. Harris, M. Low, and N. Tran, "Pileup per particle identification", *JHEP* **10** (2014) 59, doi:10.1007/JHEP10(2014)059, arXiv:1407.6013.

[65] M. Dasgupta, A. Fregoso, S. Marzani, and G. P. Salam, "Towards an understanding of jet substructure", *JHEP* **09** (2013) 029, doi:10.1007/JHEP09(2013)029, arXiv:1307.0007.

[66] A. J. Larkoski, S. Marzani, G. Soyez, and J. Thaler, "Soft drop", *JHEP* **05** (2014) 146, doi:10.1007/JHEP05(2014)146, arXiv:1402.2657.

[67] CMS Collaboration, "Jet algorithms performance in 13 TeV data", CMS Physics Analysis Summary CMS-PAS-JME-16-003, CERN, 2017.

[68] CMS Collaboration, "Identification of heavy-flavour jets with the CMS detector in pp collisions at 13 TeV", (2017). arXiv:1712.07158. Submitted to *JINST*.

[69] CMS Collaboration, "Performance of electron reconstruction and selection with the CMS detector in proton-proton collisions at $\sqrt{s} = 8$ TeV", *JINST* **10** (2015) P06005, doi:10.1088/1748-0221/10/06/P06005, arXiv:1502.02701.

[70] CMS Collaboration, "Reconstruction and identification of τ lepton decays to hadrons and ν_τ at CMS", *JINST* **11** (2016) P01019, doi:10.1088/1748-0221/11/01/P01019, arXiv:1510.07488.

[71] F. Garwood, "Fiducial limits for the poisson distribution", *Biometrika* **28** (1936) 437–442, doi:10.1093/biomet/28.3-4.437.

[72] J. Bellm et al., "Herwig 7.0/Herwig++ 3.0 release note", *Eur. Phys. J. C* **76** (2016) 196, doi:10.1140/epjc/s10052-016-4018-8, arXiv:1512.01178.

[73] M. Bähr et al., "Herwig++ physics and manual", *Eur. Phys. J. C* **58** (2008) 639, doi:10.1140/epjc/s10052-008-0798-9, arXiv:0803.0883.

[74] J. Butterworth et al., "PDF4LHC recommendations for LHC Run II", *J. Phys. G* **43** (2016) 23001, doi:10.1088/0954-3899/43/2/023001, arXiv:1510.03865.

[75] A. Kalogeropoulos and J. Alwall, "The SysCalc code: A tool to derive theoretical systematic uncertainties", arXiv:1801.08401.

[76] CMS Collaboration, "CMS Luminosity Measurement for the 2016 Data Taking Period", CMS Physics Analysis Summary CMS-PAS-LUM-17-001, CERN, 2017.

[77] T. Junk, "Confidence level computation for combining searches with small statistics", *Nucl. Instrum. Meth. A* **434** (1999) 435, doi:10.1016/S0168-9002(99)00498-2, arXiv:hep-ex/9902006.

[78] A. L. Read, "Presentation of search results: the CL_s technique", *J. Phys. G* **28** (2002) 2693, doi:10.1088/0954-3899/28/10/313.

[79] CMS and ATLAS Collaborations, "Procedure for the LHC Higgs boson search combination in Summer 2011", CMS Note CMS-NOTE-2011-005, ATL-PHYS-PUB-2011-11, CERN, 2011.

[80] G. Cowan, K. Cranmer, E. Gross, and O. Vitells, "Asymptotic formulae for likelihood-based tests of new physics", *Eur. Phys. J. C* **71** (2011) 1554, doi:10.1140/epjc/s10052-011-1554-0, arXiv:1007.1727. [Erratum: doi:10.1140/epjc/s10052-013-2501-z].

[81] D. Eriksson, J. Rathsman, and O. Stål, "2HDMC — two-Higgs-doublet model calculator physics and manual", *Comput. Phys. Commun.* **181** (2010) 189, doi:10.1016/j.cpc.2009.09.011, arXiv:0902.0851.

[82] R. V. Harlander, S. Liebler, and H. Mantler, "SusHi: A program for the calculation of Higgs production in gluon fusion and bottom-quark annihilation in the Standard Model and the MSSM", *Comput. Phys. Commun.* **184** (2013) 1605, doi:10.1016/j.cpc.2013.02.006, arXiv:1212.3249.